Environmental Modelling & Software 83 (2016) 310–325

Contents lists available at ScienceDirect

Environmental Modelling & Software

journal homepage: www.elsevier.com/locate/envsoft

Simulating the spatio-temporal dynamics of soil erosion, deposition, and yield using a coupled sediment dynamics and 3D distributed hydrologic model

Tan Zi [a], Mukesh Kumar [a, b], Gerard Kiely [c], Ciaran Lewis [c], John Albertson [a, d, *]

[a] Department of Civil and Environmental Engineering, Duke University, NC, USA
[b] Nicholas School of the Environment, Duke University, NC, USA
[c] Centre for Hydrology, Micrometeorology and Climate Change, Dept. of Civil and Environmental Engineering, University College Cork, Cork, Ireland
[d] School of Civil and Environmental Engineering, Cornell University, NY, USA

ARTICLE INFO

Article history:
Received 3 August 2015
Received in revised form
11 May 2016
Accepted 3 June 2016
Available online 25 June 2016

Keywords:
Distributed hydrologic model
Soil erosion
Sediment spatio-temporal dynamics
Coupled modeling
Sediment transport model
GEOtop model

ABSTRACT

Since soil erosion is driven by overland flow, it is fair to expect heterogeneity in erosion and deposition in both space and time. In this study, we develop and evaluate an open-source, spatially-explicit, sediment erosion, deposition and transport module for the distributed hydrological model, GEOtop. The model was applied in Dripsey catchment in Ireland, where it captured the total discharge volume and suspended sediment yield (*SSY*) with a relative bias of −1.2% and −22.4%, respectively. Simulation results suggest that daily *SSY* per unit rainfall amount was larger when the top soil was near saturation. Simulated erosion and deposition areas, which varied markedly between events, were also found to be directly influenced by spatial patterns of soil saturation. The distinct influence of soil saturation on erosion, deposition and *SSY* underscores the role of coupled surface-subsurface hydrologic interactions and a need to represent them in models for capturing fine resolution sediment dynamics.

Software availability

Software Name: GEOtopSed
Developers: Tan Zi
Contact Address: Department of Civil and Environmental Engineering, Duke University, Durham, North Carolina, 27708, US
Email: tan.zi@duke.edu
Year First Available: 2015
Hardware Required: Desktop/Laptop with 2 GHz CPU, 2 GB RAM or more
Operating System Required: Macintosh OSX 10.4 or newer; Windows XP or newer; Linux
Libraries Required: ASCII, FLUIDTURTLES, GEOMORPHOLOGYLIB, KeyPalette, MATH
Cost: Free
Source Code: https://sourceforge.net/projects/geotopero/
Program Language: C

1. Introduction

Soil erosion by rainfall and overland flow is a widespread threat to soil fertility and water quality. Accurate estimation of soil loss and its spatial distribution is often needed for pollutant risk analyses, reservoir management, agriculture productivity forecasts, and soil and water conservation. In this regard, several distributed models have been developed to obtain erosion estimates (DeRoo et al., 1996; Wicks and Bathurst, 1996; Morgan et al., 1998; Hessell, 2005; Jain et al., 2005; de Vente et al., 2008). Notably, majority of distributed erosion-deposition models e.g., WEPP, EUROSEM etc., consider simplistic representations of vertical and lateral subsurface water flow, and often do not account for the lateral subsurface water movement, or the coupled dynamic interactions between vadose zone and the groundwater table, or the evolution of soil moisture and groundwater with evapotranspiration. Given that the detachment, transport, and deposition of soil are dominantly influenced by the velocity and volume of overland flow (Julien and Simons, 1985), which in turn may be influenced by antecedent soil moisture conditions (Legates et al., 2011; Penna et al., 2011; Jost et al., 2012; Chen et al., 2014;

* Corresponding author. Department of Civil and Environmental Engineering, Duke University, NC, USA.
E-mail address: albertson@cornell.edu (J. Albertson).

http://dx.doi.org/10.1016/j.envsoft.2016.06.004
1364-8152/

Hueso-González et al., 2015), subsurface heterogeneity (Lewis et al., 2012; Ghimire et al., 2013; Orchard et al., 2013; Zimmermann et al., 2013; Niu et al., 2014; Tao and Barros, 2014), and groundwater distribution (Kumar et al., 2009; Miguez-Macho and Fan, 2012; Rosenberg et al., 2013; Safeeq et al., 2014; von Freyberg et al., 2015), it is important to consider the coupled impacts of antecedent hydrologic states (soil moisture and groundwater distribution) and subsurface hydrogeologic properties on sediment generation and yield. Failing to do so may limit the applicability of these models to a few events (Hessel et al., 2006; Mati et al., 2006; Ramsankaran et al., 2013) or to regimes where the dynamic role of antecedent conditions and subsurface heterogeneity on erosion are not large enough. Heppner et al. (2006) made significant headway in this direction by coupling sediment processes within an integrated hydrologic model, InHM (VanderKwaak and Loague, 2001). The study specifically evaluated the rainfall splash erosion component of the model on a 6 m by 2.4 m plot. Heppner et al. (2007) used the same model to perform sediment-transport simulations for six events in a 0.1 km^2 rangeland catchment. It is to be noted that InHM solves subsurface flow using the variably saturated 3D-Richards equation, while surface flow is simulated using diffusion wave approximation of St. Venant equation. Equations corresponding to these coupled processes are spatially discretized using a control volume finite element strategy on each unstructured grid. A global implicit solver is used to perform the simulation. Another notable effort in this direction was by Kim et al. (2013), who coupled sediment processes within a hydrologic and hydrodynamic model tRIBS-OFM and validated their model against analytical solutions. Similar to InHM, tRIBS-OFM is also an unstructured grid based model. The model uses a gravity-dominated formulation (Cabral et al., 1992) to simulate vadose zone flow and a quasi-3D Boussinesq's equation under the Dupuit-Forchheimer assumptions to simulate groundwater flow (Ivanov et al., 2004). The model was used to evaluate sediment yield simulations for 10 events in a 0.036 km^2 Lucky Hills watershed located in southeastern Arizona, USA. Development of these physically-based integrated models of hydrology and sediment dynamics has opened new opportunities, especially in regards to understanding the impact of the hydrologic state on spatio-temporal distribution of erosion, deposition and yield. Notably, the aforementioned two models are not open-source.

Here, we develop an open-source, spatially-explicit, structured-grid based, sediment erosion/deposition module for a 3D surface-subsurface hydrologic model, GEOtop (Rigon et al., 2006; Endrizzi et al., 2014), and evaluate its applicability in explaining the sediment yield dynamics. Similar to InHM (Heppner et al., 2007), the GEOtop model also solves subsurface flow using the variably saturated 3D-Richards equation, while surface flow is simulated using kinematic wave approximation of St. Venant equation. The sediment dynamics model developed here takes advantage of the GEOtop simulated distributed hydrological states such as moisture content, surface flow depth, and flow velocity. The model accounts for the influence of spatial heterogeneities in land surface characteristics, subsurface hydrogeology, and antecedent conditions in the generation of overland flow, and hence on the erosion and deposition of sediment in the catchment. The model developed here was applied on a much larger catchment (area = 15 km^2) and for a longer period (simulation duration = 2 years) than in Heppner et al. (2007) and Kim et al. (2013), allowing validation of the coupled model for extended wet and dry periods. The coupled model is then used synergistically with the observed data to answer four pointed questions: a) Is the performance of the GEOtopSed model for simulating *SSY*, dependent on the flow regime and the model's ability to capture streamflow response? b) Does the daily suspended sediment yield (*SSY*) from the watershed vary monotonically with precipitation amount and energy? If not, does the hydrologic response of the watershed has a role to play in the departure from monotonic relation? c) Does the simulated source/sink area of sediments vary spatially from one event to other? If yes, is the variation driven by hydrologic state, specifically the surface soil saturation state? and d) To what extent does the linear relation between erosion and the slope-length factor (product of specific catchment area and slope), which is often used in USLE-based model representations (e.g. USLE (Wischmeier and Smith, 1978), RUSLE (Renard et al., 1991), RUSLE2 (Foster et al., 2005)), hold for GEOtopSed simulated states and fluxes?

2. Process formulation, model implementation, and verification

2.1. The GEOtop model: a short review

The open-source GEOtop model (Rigon et al., 2006) is process based and simulates core hydrological processes such as unsaturated flow, saturated flow, overland flow, stream flow generation/routing, and surface energy balances. Overland flow modeling is performed using the kinematic wave approximation of St. Venant equation while subsurface flow and soil moisture simulations are performed by solving a variably-saturated representation of 3D Richards equation. By solving the Richards equation, GEOtop model can simulate the surface runoff generation processes due to both infiltration excess and saturation excess, and can also redistribute the sub-surface water both laterally and vertically, as determined by the head gradient. The model has been extensively tested and validated in Bertoldi (2004). The water and energy balance calculations in GEOtop were recently refined to account for soil freezing and thawing effects (Endrizzi et al., 2014). In summary, with detailed water and energy balance modules, GEOtop can provide accurate simulations of evapotranspiration and soil moisture dynamics (Bertoldi et al., 2014; Della Chiesa et al., 2014), given adequate watershed data. By simulating coupled hydrologic states (e.g. surface flow depth, soil moisture and groundwater) on each grid of the model domain, the model is well suited to study the influence of watershed properties and subsurface states on spatially-distributed runoff, an important control on erosion, at multiple scales. Furthermore, as an open source software (http://www.geotop.org/wordpress/), the GEOtop model provides a complete hydrological model framework with ease for extensions. One such example is the incorporation of landslide occurrence prediction within the GEOtop framework by Simoni et al. (2008).

2.2. Process formulation of the sediment dynamics model

The sediment dynamics model developed here takes advantage of the GEOtop simulated distributed hydrological states such as moisture content, surface flow depth, and flow velocity. Here we only highlight the aspects of the model that are most relevant to the sediment erosion, deposition and transport modeling. Readers may refer to GEOtop model papers (Rigon et al., 2006; Endrizzi et al., 2014) to learn more about the individual process representations.

GEOtop simulates soil moisture in each subsurface layer by solving the 3D Richards equation:

$$(C(H)\phi + S_w S_s)\frac{\partial H}{\partial t} + \nabla\cdot(-\mathrm{K}\nabla\mathrm{H}) + S_w = 0 \quad (1)$$

where K [m s^{-1}] is the hydraulic conductivity, H [m] is the sum of pressure and potential head, and S_w is the source/sink mass flux [s^{-1}], S_s is the specific storage coefficient [m^{-1}], ϕ is porosity [−], and $C(H)$ is the specific moisture capacity function.

Surface overland flow is routed along the flow direction using kinematic wave approximation of the Saint-Venant equation represented as:

$$\frac{\partial h}{\partial t} + \frac{\partial q}{\partial x} = q_L \tag{2}$$

where h is depth of overland flow [m], x is a local coordinate system oriented along the flow direction [m]; q is flow rate per unit width [$m^2\ s^{-1}$], and q_L is vertical inflow or outflow rate (to the surface water) per unit area [$m\ s^{-1}$]. The flow direction is defined along the line of steepest downslope head gradient between the grid and its eight neighbors. The overland flow equation is coupled to the continuity equation of sediment transport at each time step using:

$$\frac{\partial hC}{\partial t} + \frac{\partial qC}{\partial x} = E_x \tag{3}$$

where C is sediment concentration in the overland flow within each cell [$kg\ m^{-3}$], and E_x is the exchange rate of sediment per unit surface area [$kg\ m^{-2}\ s^{-1}$] at the interface of soil and water. E_x is composed of three major mechanisms: rainfall splash detachment (D_R), flow detachment (D_F) and deposition (D_P), as:

$$E_x = D_R + D_F - D_P. \tag{4}$$

D_R [$kg\ m^{-2}\ s^{-1}$] is approximated by DeRoo et al. (1996):

$$D_R = \left(0.1033\frac{Ke}{\zeta}e^{-1.48h} + 3.58\right)*I \tag{5}$$

where ζ is soil cohesion [kPa], Ke is rainfall kinetic energy [$J\ m^{-2}\ mm^{-1}$], and I is the precipitation intensity [$mm\ h^{-1}$]. D_F and D_P [$kg\ m^{-2}\ s^{-1}$] are related to transport capacity (T_C) based on the erosion-deposition theory proposed by Smith et al. (1995).

$$D_F = (T_C - C)*y*v_s \tag{6}$$

$$D_P = (T_C - C)*v_s \tag{7}$$

where y is an efficiency coefficient that is a function of soil cohesion (DeRoo et al., 1996), and v_s is settling velocity of the particles [$m\ s^{-1}$]. The dependence of soil cohesion on soil moisture (Bullock et al., 1988) and root tensile strength (Wu et al., 1979) is captured using:

$$\zeta_s = \left(\frac{\theta}{\theta_s}\right)^2 \zeta_{ss} \tag{8}$$

$$\zeta_{add} = 1.2*R_S \tag{9}$$

$$\zeta = \zeta_{add} + \zeta_s \tag{10}$$

where ζ_s, ζ_{ss}, ζ_{add} are bare soil cohesion, saturated bare soil cohesion and additional cohesion by roots respectively, θ and θ_s are the soil moisture and saturated soil moisture contents respectively, and R_S is the root total tensile strength [kPa]. The transport capacity is based on the experiments conducted by Govers (1990):

$$T_C = a(\omega - \omega_{cr})^b*\rho \tag{11}$$

where ω is the unit stream power [$m\ s^{-1}$] (Yang, 1972), ω_{cr} is the critical power that initiates flow detachment of soil particles [$m\ s^{-1}$], ρ is the density of soil particles [$kg\ m^{-3}$], and a and b are empirical parameters related to soil particle size.

The sediment mass balance in each stream channel reach was calculated using:

$$\frac{\partial \boldsymbol{h_c C_c}}{\partial \boldsymbol{t}} + \frac{\partial \boldsymbol{q_c C_c}}{\partial \boldsymbol{x}} = \boldsymbol{I_n} \tag{12}$$

where q_c is the discharge per unit width in channel [$m\ s^{-1}$], h_c is the water depth of channel [m], C_c is sediment concentration in channel [$kg\ m^{-3}$], and I_n is the sediment exchange rate per unit area between adjacent land cells and the channel cell [$kg\ m^{-2}\ s^{-1}$]. The suspended sediment yield (SSY) [kg] at the outlet of the catchment was the integration of suspended sediments over the period of interest:

$$SSY = \int Q_{ol}C_{ol}dt \tag{13}$$

where Q_{ol} is the discharge rate at outlet [$m^3\ s^{-1}$], C_{ol} is the sediment concentration at the outlet cell [$kg\ m^{-3}$] and dt is an hourly integration time step. The period of integration in the ensuing analyses varied from hourly to annual scale and has been appropriately identified at relevant locations.

2.3. Model implementation

The GEOtop model first solves the finite difference discretization of 3D Richards equation (Equation (1)) using Bi-conjugate gradient stabilized method (Vorst, 1992). An absolute numerical tolerance of 10^{-4} mm is used for ensure water balance. This requires performing simulations at an adaptive time-step with time intervals generally ranging from minutes to hours. After solving the 3D Richards equation, H in the top layer is used to calculate the head gradient for estimation of infiltration/exfiltration flux in Equations (1) and (2), at a user defined interval (hourly in this study). Finite difference discretization of the surface flow, channel routing, and sediment transport equations (Equations (2), (3) and (12)) are then solved altogether using a forward explicit Euler method. To ensure stability, Courant-Friedrichs-Lewy (CFL) condition is used. The Courant number is set to 0.25. If the CFL condition is not satisfied, the time step is reduced by 75% adaptively until it gets satisfied. Although the integrated model simulations are performed using an adaptive time-stepping scheme, the model outputs are printed at constant intervals.

2.4. Model verification at plot scale

GEOtopSed was first evaluated on a soil flume setup discussed in Ran et al. (2012). The setup included a rainfall simulator, a tilted soil flume, an overland flow collector, and a set of soil water content monitor devices. The rainfall simulator was used to generate rain events of varying intensity, duration, moving direction, rainfall position, and no-rainfall interval. The size of the soil flume was 5 m long by 1 m wide. In the flume, a 30 cm thick soil layer with a fixed slope of 25°, and containing 13% clay, 58% silt, and 29% sand was set on top of a 5 cm thick sand layer. Surface runoff and sediment were collected at the end of the soil flume in a metal container placed slightly below the soil surface. All other boundaries of the soil flume were impermeable. Readers are referred to Ran et al. (2012) to learn more about the experimental setup. The model simulations were performed on a grid discretization with a resolution of 1 m × 1 m × 10 cm in x, y and z directions. The model results were output at 3 min interval in this experiment.

Out of 33 rainfall scenario experiments discussed in Ran et al. (2012), here we summarize the results for three scenarios (No.10, No.14, and No.18) with markedly different rainfall intensities (Table 1). For scenario 10 (Fig. 1) which included rain events of

highest rainfall intensity (>80 mm/h) and shortest duration among the three selected scenarios, the model was able to capture the observed timing of both flow and SSC peaks. Observed flow peaks were also captured accurately. Further analyses of simulation results suggest that a smaller runoff peak for the first event, even though the duration and intensity of all the precipitation events were almost identical, was because of drier antecedent soil moisture conditions in the top soil layer. Once the moisture deficit of top layer is fulfilled, additional precipitation contributes to infiltration-excess runoff even while the lower soil layers are not yet saturated. Since the second event occurred only 0.25 h after the first one, the top soil layer was still near saturation resulting in a larger runoff peak than the first event. For later events, several model cells were fully saturated i.e. all vertical layers were saturated, indicating that both infiltration-excess and saturation-excess processes played a role in generation of runoff peaks for these events. The model was also able to capture the relatively smaller runoff peak magnitude in scenarios 14 and 18 due to the reduced intensity of events. Overall, the timing of simulated SSC peaks also matched the peak in observed records. For scenarios 10, the model was able to capture the magnitude and the decreasing trend in SSC for events 2 to 5. The first simulated SSC peak was however underestimated. Analyses of simulated states suggest that the decreasing trend in SSC may be explained based on the combined effects of increase in flow volume which reduces SSC, reduction in sediment generation with small decrease in peak flow, and an increase in soil cohesion with increasing soil moisture which impedes sediment generation. For scenario 14, the model was again able to capture the decreasing trend in SSC for the four events. In scenario 18, the SSC was measured only for two events as the first precipitation pulse did not generate any response. The model captured the magnitude of runoff peak corresponding to the third event, but underestimated for the second event. It is to be noted that the runoff generated for the second event is negligible and SSC estimates are very sensitive at these magnitudes.

In summary, the GEOtopSed model generally captured both the trend and the quantity of runoff and suspended sediment concentration (SSC). It is to be noted that an accurate simulation of runoff and consequently of SSC was possible because of comprehensive representation of surface and subsurface hydrological processes in the model.

3. Model application at watershed scale

3.1. Site description

The coupled model was applied at a small experimental catchment, in Dripsey, Ireland (Fig. 2). Given that groundwater and antecedent soil moisture have been found to play an important role on runoff generation (Lewis et al., 2013) and nutrient transport (Warner et al., 2009) in the catchment, the site serves as a good test case for validating the integrated model at catchment scale. The Dripsey catchment is located approximately 25 km northeast of Cork, and has an area of 15 km^2. The elevation of this catchment ranges from 60 to 210 m. It is a beef and dairy producing agricultural catchment and is almost 100% covered by perennial ryegrass. The catchment slopes gently, with around 85% of the area having less than 3% grade. Gleys and podzols are the two major soil types. The experimental field site is managed by the Hydromet team of the University College Cork (UCC). There is a meteorological flux tower at the top of the catchment (elevation 192 m) where radiation, wind speed, air temperature, surface temperature, relative humidity, and soil moisture (at five depths) have been measured at 30 min interval since 1998 (Albertson and Kiely, 2001). All the meteorological data from the site are archived in the FLUXNET repository (http://fluxnet.ornl.gov). At the catchment outlet (elevation 60 m), stream flow was monitored continuously at 30 min interval for a period of over two years (2002–2003). Flow-weighted water samples at the catchment outlet were collected using an ISCO 6712 auto-sampler with intake set at approximately 0.25 m above the streambed (Lewis, 2003, 2011).

The climate in the study region is temperate maritime, and is characterized by high humidity and a lack of temperature extremes during the year. The minimum daily temperature for years 2002 and 2003 was −0.2° C. The mean annual precipitation locally is approximately 1400 mm. The annual precipitation in the Dripsey catchment for year 2002 and 2003 was 1823 mm and 1178 mm, respectively. Winter and spring were the wetter seasons while summer was generally dry (Fig. 3). No precipitation was recorded during the period with temperature below 0 °C during the two years. Suspended sediment losses over the catchment were estimated from measured data of stream flow volume and suspended sediment concentration. The monthly variations in suspended sediment yield are shown in Fig. 3. Notably, the runoff ratio in January 2003 is larger than one. This indicates that antecedent groundwater recharge participated in delayed streamflow response in this month. Marked variations in runoff ratio through the year underscores the need for appropriate partitioning of the water budget across different stores of the hydrologic continuum.

3.2. Input data

GEOtop requires a digital elevation model (DEM), land use/land cover (LULC) map, and soil type map to simulate the hydrological processes for a catchment. The soil type map and soil parameters were obtained from Irish Forestry soils (IFS) database and *in situ* soil

Table 1
Summary of plot experiment. The experiment data are from Ran et al. (2012). Numbers in the parenthesis are simulation results from GEOtopSed.

Scenario no.	Event	Rainfall intensity (mm/h)	Rainfall amount (mm)	Rainfall duration (h)	No-rainfall interval (h)	Time of runoff peak (h)	Runoff peak (ml/s)	SSC (kg/m^3)
10	US001	83.99	21.00	0.25	0	0.12 (0.15)	30.2 (31)	57.08 (25.6)
	US002	84.42	21.10	0.25	0.25	0.09 (0.15)	38.8 (41)	30.05 (32.6)
	US003	85.05	21.26	0.25	0.5	0.20 (0.25)	40 (40)	19.53 (32.7)
	US004	86.08	21.52	0.25	1	0.12 (0.15)	38.9 (35)	14.30 (24.2)
	US005	83.80	20.95	0.25	3	0.18 (0.15)	40.8 (36)	10.63 (20.3)
14	UM001	59.15	29.57	0.5	0	0.24 (0.4)	13.6 (17)	69.35 (89.4)
	UM002	59.28	29.64	0.5	0.5	0.27 (0.3)	21.95 (21)	36.76 (33.4)
	UM003	59.47	29.73	0.5	1	0.21 (0.3)	22.4 (23)	24.20 (18.3)
	UM004	61.09	30.54	0.5	3	0.27 (0.5)	21.45 (20)	16.78 (18.7)
18	UW001	29.63	29.63	1	0	0.00 (0)	0 (0)	0.00 (0)
	UW002	23.45	23.45	1	1	0.27 (0.65)	0.233 (1)	4.77 (0.001)
	UW003	34.35	34.35	1	3	0.33 (0.65)	7.5 (11)	6.71 (6.38)

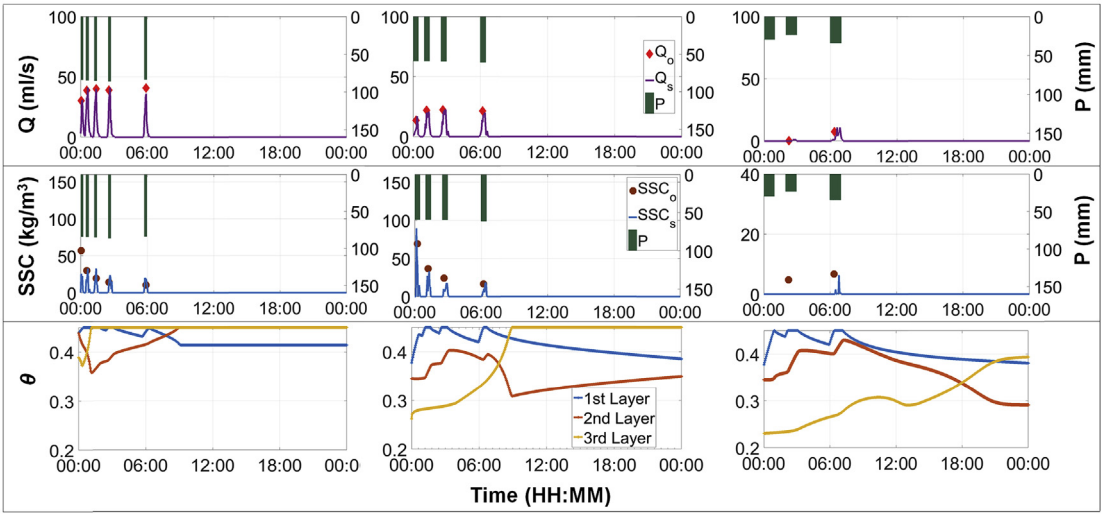

Fig. 1. Modeled and observed records for rainfall scenarios 10 (left column), 14. (middle column), and 18 (right column). The first row are the time series of precipitation and surface runoff; the second row are time series of precipitation and suspended sediment concentration (SSC); and the third row are time series of plot-average soil moisture of three subsurface layers. In the top two rows, precipitation (P) is plotted on the secondary axis.

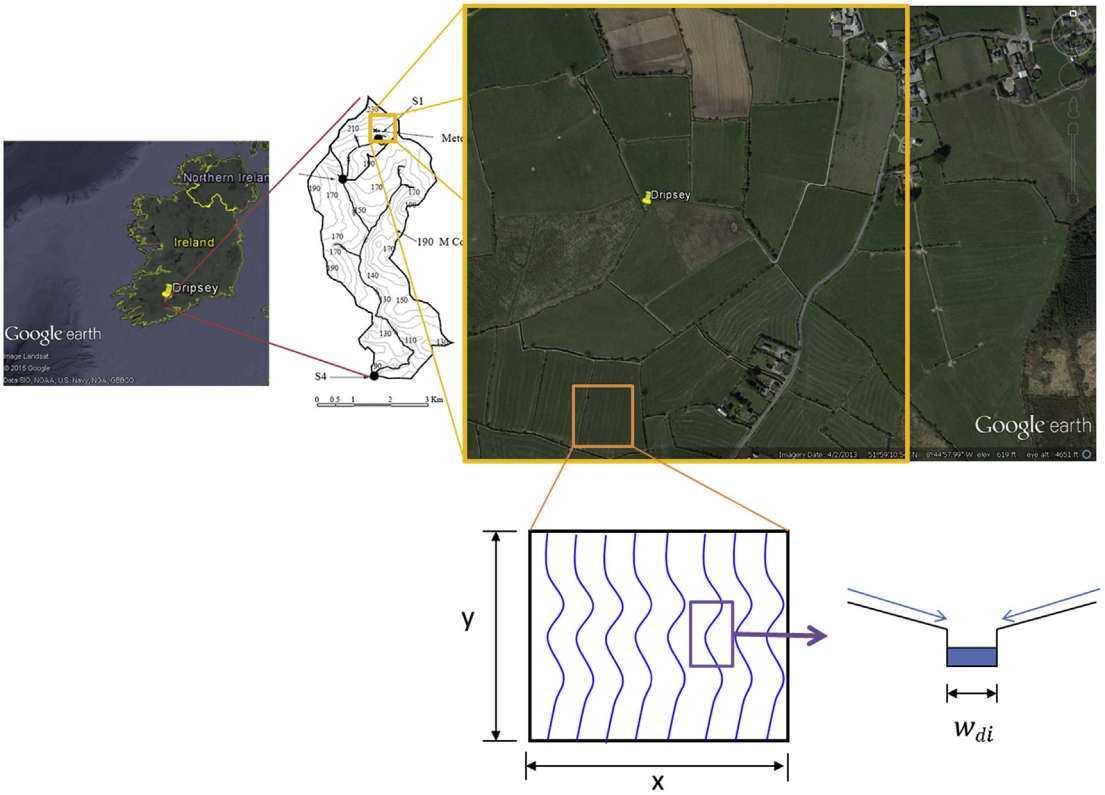

Fig. 2. Location of Dripsey catchment in County Cork, Ireland. The location of the meteorological tower is where "Dripsey" is marked in yellow. The right top panel is the Google Earth image of Dripsey catchment. The lower panel shows the conceptualization of rills (discussed in Section 3.3).(For interpretation of the references to colour in this figure legend,the reader is referred to the web version of this article.).

samples (Lewis, 2011). LULC parameters were derived based on classifications using the Corine land cover 2000 database and land use data observed in the catchment. The stream channel was delineated using DEM processing in GIS. The derived extent of stream was validated against the regional channel map. Geomorphic properties of the channel were defined based on the DEM data. All thematic maps were resampled at 50 m × 50 m spatial resolution. Meteorological data such as precipitation, temperature, incoming shortwave radiation, air pressure, relative humidity, wind speed and direction in half-hourly time steps were collected at the HYDROMET flux tower at Dripsey. Because of the small size of the catchment (area = 15 km^2) and absence of any other precipitation data fine enough to resolve the heterogeneities within the watershed, the rainfall was assumed to be uniform within the catchment.

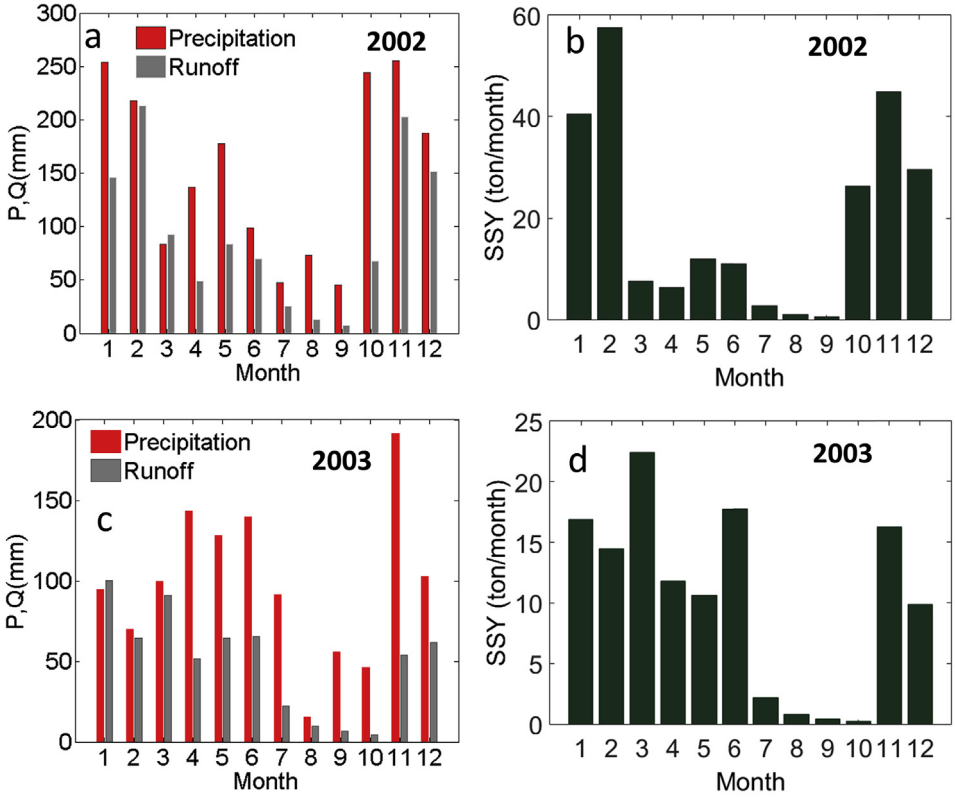

Fig. 3. Observed monthly variations in precipitation (P), discharge volume (Q) and suspended sediment losses (*SSY*) in the Dripsey catchment.

The assumption is reasonable given the mild topographic relief and a uniform land cover within the catchment. The stream flow and suspended sediment concentration data, collected by the water level recorder and water ISCO 6712 auto-sampler at the outlet of catchment, were used to both calibrate and validate the model.

3.3. Model implementation in dripsey catchment

The integrated model simulations were performed at 50 m × 50 m spatial resolution. Simulation results were output at hourly temporal resolution. While overland flow (from either saturation excess or infiltration excess) is generated over the entire land surface cell in the original GEOtop model, a rill width ratio (w_{dx}) parameter was introduced in the sediment dynamics model to account for the flow organization within each cell. The assumption here is that the generated overland flow is transferred into small rills (Fig. 2) in which overland flow gets concentrated and the potential of rill erosion is high. The rill width ratio (w_{dx}) was calculated using the following equation:

$$w_{dx} = \frac{\sum_i w_{di}}{x_w} \tag{14}$$

where i is the rill index within a cell, w_{di} is the width of ith rill [m], and x_w is the width of the cell [m]. In other words, w_{dx} is the fraction of a grid cell covered by overland flow, when overland flow is active. The soil erosion calculations were accordingly modified to account for erosion under a redistributed overland flow regime. Rain splash detachment occurred in the entire cell while the flow detachment only occurred within the rills. While rill characteristics can be observed, the absence of relevant data for the site leads us to consider rill characteristics as a calibration parameter. This is an important area for future research attention.

The model accounts for erosion, deposition, and transport of suspended sediment on the hillslopes. However, considering that the bank and bed erosion and deposition in first order river channels are not significant (Golubev, 1982), these processes were not included in sediment dynamics calculations in the channel. All the sediment entering the channels was assumed to directly reach the outlet of the watershed. It is to be acknowledged that this assumption may cause bias in suspended sediment yield estimates, especially from large basins wherein river beds and banks can be a significant source and/or sink of sediment.

3.4. Sensitivity analysis

A global multivariate sensitivity analyses was first conducted to evaluate the role of physics-based parameters that may impact soil erosion and deposition. The methodology is based on a Monte Carlo framework, and can be used to analyze the influence of a parameter while also considering the influence of all other parameters at the same time (Franks et al., 1997). The parameters chosen for the sensitivity analysis included hydrologic properties that may influence runoff generation (Table 2) and land properties that may influence soil erodibility (Table 3). Ranges of some of the soil parameter such as saturated conductivity for different layers (K), soil residual water content (θ_r), wilting point (θ_w), field capacity (θ_{fc}), saturated water content (θ_s), and soil median particle size (D_{50}) were assigned based on the sand-silt-clay fraction of *in situ* soil samples (Lewis, 2011). The *LAI* range was assigned based on the land cover of the catchment. Other parameters (Table 2, Table 3), such as Chezy's roughness coefficient (C_m), rill width ratio (w_{dx}), and root area ratio (R_a) were assigned a conservative range large enough to encompass the range of parameters used in previous studies. Model simulations were conducted using a single rainfall event for 10,000 random sets of parameters, which were sampled

Table 2
Ranges and numerical sensitivity index (*NSI*) of hydrologic parameters.

Variable name	Description	Range	*NSI*
LAI	Leaf area index	0.1–4	0.073
C_F	Canopy fraction	0–1	0.0009
C_m	Chezy's roughness coefficient	0.01–5	0.0325
w_{dx}	Rill width ratio	0.01–1	0.073
D_1 [mm]	Soil depth of first layer	25–300	0.0731
K_{h_L1} [mm s^{-1}]	Horizontal saturated conductivity (1st layer)	0.00036–0.12	0.0008
$Kv_{\_L1}$ [mm s^{-1}]	Vertical saturated conductivity (1st layer)	0.00036–0.06	0.0322
θ_{r_L1}	Residual water content (1st layer)	0.03–0.06	0.0033
θ_{w_L1}	Wilting point (1st layer)	0.06–0.16	0.0040
θ_{fc_L1}	Field capacity (1st layer)	0.3–0.5	0.0050
θ_{s_L1}	Saturated water content (1st layer)	0.3–0.6	0.0045
K_{h_L2} [mm s^{-1}]	Horizontal saturated conductivity (2nd layer)	0.00036–0.12	0.0012
$Kv_{\_L2}$ [mm s^{-1}]	Vertical saturated conductivity (2nd layer)	0.00036–0.06	0.0001
θ_{r_L2}	Residual water content (2nd layer)	0.03–0.06	0.0035
θ_{w_L2}	Wilting point (2nd layer)	0.06–0.16	0.0006
θ_{fc_L2}	Field capacity (2nd layer)	0.3–0.5	0.0013
θ_{s_L2}	Saturated water content (2nd layer)	0.3–0.6	0.0062
K_{h_L3} [mm s^{-1}]	Horizontal saturated conductivity (3rd layer)	0.00036–0.12	0.0076
$Kv_{\_L3}$ [mm s^{-1}]	Vertical saturated conductivity (3rd layer)	0.00036–0.06	0.0119
θ_{r_L3}	Residual water content (3rd layer)	0.03–0.06	0.0026
θ_{w_L3}	Wilting point (3rd layer)	0.06–0.16	0.0006
θ_{fc_L3}	Field capacity (3rd layer)	0.3–0.5	0.0048
θ_{s_L3}	Saturated water content (3rd layer)	0.3–0.6	0.0005

Table 3
Ranges and numerical sensitivity index (*NSI*) of erosion and sediment dynamics parameters.

Variable name	Description	Range	*NSI*
C_m	Chezy's roughness coefficient	0.01–5	0.3569
R_s [MPa]	Root tensile strength	0.001–0.1	0.0236
R_a	Root area ratio	0.001–0.1	0.0033
w_{dx}	Rill width ratio	0.01–1	0.3569
D_{50} [μm]	Median particle size	5–200	0.3563
ζ [kPa]	Soil cohesion	0–30	0.0237

from uniform distributions across the specified parameter ranges. Based on the rank of Nash-Sutcliffe coefficients (*NSE*) for each parameter set, the 10,000 parameter sets were divided into ten performance classes, each with 1000 parameter sets. The classes were ranked by *NSE* from low to high, i.e. Class 1 consisted of parameter sets with lowest *NSE* while Class 10 comprised of parameter sets with highest *NSE*. A numerical sensitivity index (*NSI*) was used to quantify the sensitivity (Montaldo et al., 2003):

$$NSI = \frac{1}{n_c N x_{range}} \sum_{i=1}^{n_c} \sum_{j=1}^{N} x_d(i,j) \tag{15}$$

where x_d is the difference between the parameter values of two classes for the jth cumulative frequency and for ith pair of cumulative frequency curves, n_c is the total number of pairs of cumulative frequency classes (with 10 classes, $n_c = 45$), and N is the number of cumulative frequency values in each performance class ($N = 1000$ in this case). x_{range} is the range of parameter values. *NSI* is an indicator of the distance between each class. A larger value of *NSI* for a parameter indicates higher sensitivity to it. It is to be noted that while generating the parameter sets, extra care was taken to ensure that the considered values of dependent parameters were physically realistic. For example, only the parameter sets with soil residual water content (θ_r), wilting point (θ_w), field capacity (θ_{fc}) and saturated water content (θ_s) in increasing order were considered. It is also possible that only certain ranges of parameters may co-exist. However, because of the absence of any parameter-concurrency data for the region, the sensitivity analyses did not consider this.

The sensitivity of hydrologic and land surface parameters is presented individually here. Among the 23 parameters selected for the hydrological sensitivity analysis, leaf area index (*LAI*), rill width ratio (w_{dx}), depth of the first soil layer (D_1), Chezy's roughness coefficient (C_m), and vertical hydraulic conductivity of the first soil layer (K_{v_L1}) were found to be among the five most sensitive parameters for runoff generation (Table 2). Similarly, C_m, w_{dx} and D_{50} were observed to be the three most sensitive parameters for sediment yield simulations (Table 3). Root tensile strength (R_s) and soil cohesion (ζ) also were important players in sediment yield simulations, though to a lesser extent than the other three parameters identified above. Among the three most sensitive parameters for sediment yield, D_{50} can be estimated from soil texture and C_m can be related to land cover and land use. w_{dx} can be highly varied between different watersheds or land parcels depending on microtopographic heterogeneity arising from natural causes or implementation of agricultural practices (e.g. tillage farming). The other two sensitive parameters for sediment yield simulations: root tensile strength (R_s) and soil cohesion (ζ), are correlated, as R_s proportionally affects ζ (see Equations (7)–(9)) and both the parameters have a tendency to reduce soil erosion.

Having identified the most sensitive parameters, next a univariate sensitivity experiment was performed to investigate the role of two sensitive but independent parameters (w_{dx} and ζ) on erosion simulations. This involved forcing the model with a 32 mm precipitation event of 24 h duration. As shown in Fig. 4, increasing w_{dx} caused a reduction in suspended sediment losses. This is because for a wider rill, overland flow depth and velocity is smaller resulting in a smaller shear stress between water and soil surface to detach the soil particles. It is to be noted that the relative changes in w_{dx} (base value equals to 0.5) were larger than the relative changes in *SSY*. For example, 20% decrease in w_{dx} increased sediment yield by 15%. This was due to the offset effect of reduction in flow detachment area when the rills are narrower.

Five additional sensitivity experiments with varying rainfall intensities, but with identical precipitation amount, were conducted to evaluate potential controls of event characteristics on the sensitivity of sediment yield to w_{dx}. Different rainfall intensities did not show significant impacts on sensitivity analysis, indicating that flow detachment rather than splash erosion, was the major driving

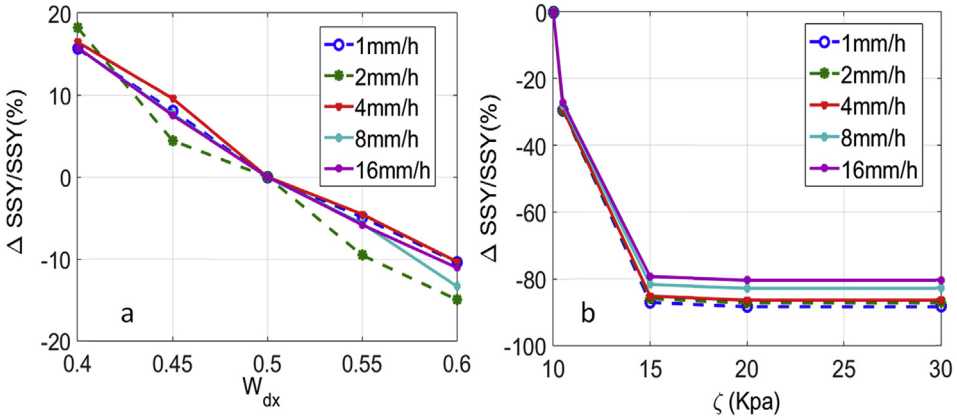

Fig. 4. Sensitivity of rill width ratio, w_{dx} (a) and soil cohesion, ζ (b) on suspended sediment yield (*SSY*) for a range of precipitation intensities.

force for water erosion in Dripsey catchment. This is possibly caused by the dense grassland vegetation cover within Dripsey catchment which protected the soil surface from detachment by raindrops. Similar sensitivity experiment for soil cohesion (ζ) showed that the sediment yield decreased with increase in ζ. The influence of soil cohesion on erosion was the largest when cohesion value was between 10 and 20 kPa. Notably, as the precipitation intensity increased, the sensitivity to soil cohesion decreased.

It is to be noted that sediment yield simulations could be influenced both by parameters that control rainfall-runoff processes and parameters that define the land surface and soil characteristics. This makes calibration of a physically based integrated erosion-deposition models much more challenging than integrated hydrologic models.

3.5. Model performance during calibration and validation periods

3.5.1. Evaluation metrics

Performance of the model was evaluated using four metrics: Relative bias (*RB*), Nash–Sutcliffe efficiency (*NSE*), index of agreement (*IOA*), and Root mean square error (*RMSE*). *RB* evaluates the relative distances between observed (O) and simulated (S) data with respect to the observed mean ($\overline{O}$) using:

$$RB = 100\frac{\sum_{i=1}^{n}(S_i - O_i)}{n\overline{O}} \tag{16}$$

where n is the length of data series. *NSE* (Nash and Sutcliffe, 1970) is a dimensionless goodness-of-fit indicator that ranges from negative infinity to one. A *NSE* value of 1 indicates a perfect fit between observed and simulated data.

$$NSE = 1 - \frac{\sum_{i=1}^{n}(O_i - S_i)^2}{\sum_{i=1}^{n}\left(O_i - \overline{O}\right)^2}. \tag{17}$$

In the context of watershed hydrologic modeling, Moriasi et al. (2007) summarized that the model performance could be considered as "Good" if the *RB* is less than 15% for streamflow and 30% for sediment, and *NSE* is larger than 0.65 for monthly time step simulations. For finer time step, the equivalent "goodness" threshold of *NSE* is lower, e.g. *NSE* value of 0.65 for monthly time step may yield a *NSE* value of 0.4 for daily time step (Fernandez et al., 2005). *IOA* (Willmott, 1981) is used to detect the differences in the observed and simulated means and variances, especially during the intense rainfall events as the metric is sensitive to extreme values. *IOA* ranges from 0 to 1. A value of 1 indicates a perfect match, and 0 indicates no agreement at all. Krause et al. (2005) concluded that *IOA* of 0.65 could indicate a good model performance, although *IOA* is not sensitive to systematical under- or over-estimation:

$$IOA = 1 - \frac{\sum_{i=1}^{n}(O_i - S_i)^2}{\sum_{i=1}^{n}\left(|S_i - \overline{O}| + |O_i - \overline{O}|\right)^2}. \tag{18}$$

RMSE quantifies prediction error as:

$$RMSE = \sqrt{\frac{\sum_{i=1}^{n}(O_I - S_i)^2}{N}}. \tag{19}$$

A *RMSE* value of zero indicates perfect fit. If the value is less than half of the standard deviation of the observations, the model performance may be considered as good (Singh et al., 2005).

3.5.2. Calibration period

The calibration was carried out using hourly flow data and suspended sediment concentration data from Jan 1st, 2002 to Mar 14th, 2002 (73 days, 10% of the observed data). The GEOtopSed model spin-up was performed using the meteorological data of Dec 2001. The calibration process mainly focused on the most sensitive parameters, as identified in the global sensitivity analyses. C_m, D_1, and w_{dx} were the three major parameters calibrated for the flow simulation. ζ and D_{50} were mainly calibrated for erosion simulation. The initial values of the calibration parameters were set to the median of the ranges in Tables 2 and 3. The model calibration was based on both mass balance and goodness of fit of hydrograph and sedigraph. The goal was to at least limit the relative bias (*RB*) of total discharge volume and total *SSY* to less than 15% and to have *NSE* of daily average flow rate and daily total *SSY* to be larger than 0.4.

The observed and simulated stream flow series in calibration period are shown in Fig. 5a and b. Observed and simulated total discharge volumes per unit area over the calibration period were 411 mm and 472 mm, respectively (*RB* ~ 15%). The R^2 and Nash-Sutcliff coefficient (*NSE*) were 0.76 and 0.48, respectively. The index of agreement (*IOA*) was 0.92 and the root mean square error (*RMSE*) was 3.03 mm/day. The *NSE, IOA,* and *RB* values indicate a "good" model performance based on the threshold proposed by Moriasi et al. (2007) and Krause et al. (2005). The *RMSE* was 71% of the standard deviation of observed streamflow, which means that the model performance was not good (Singh et al., 2005). Large *RMSE* value is because of the model's tendency to overestimate high flow and underestimate low flow (Fig. 5b).

In regards to the estimates of suspended sediment yield (*SSY*), the model also showed good agreement with the observations. The

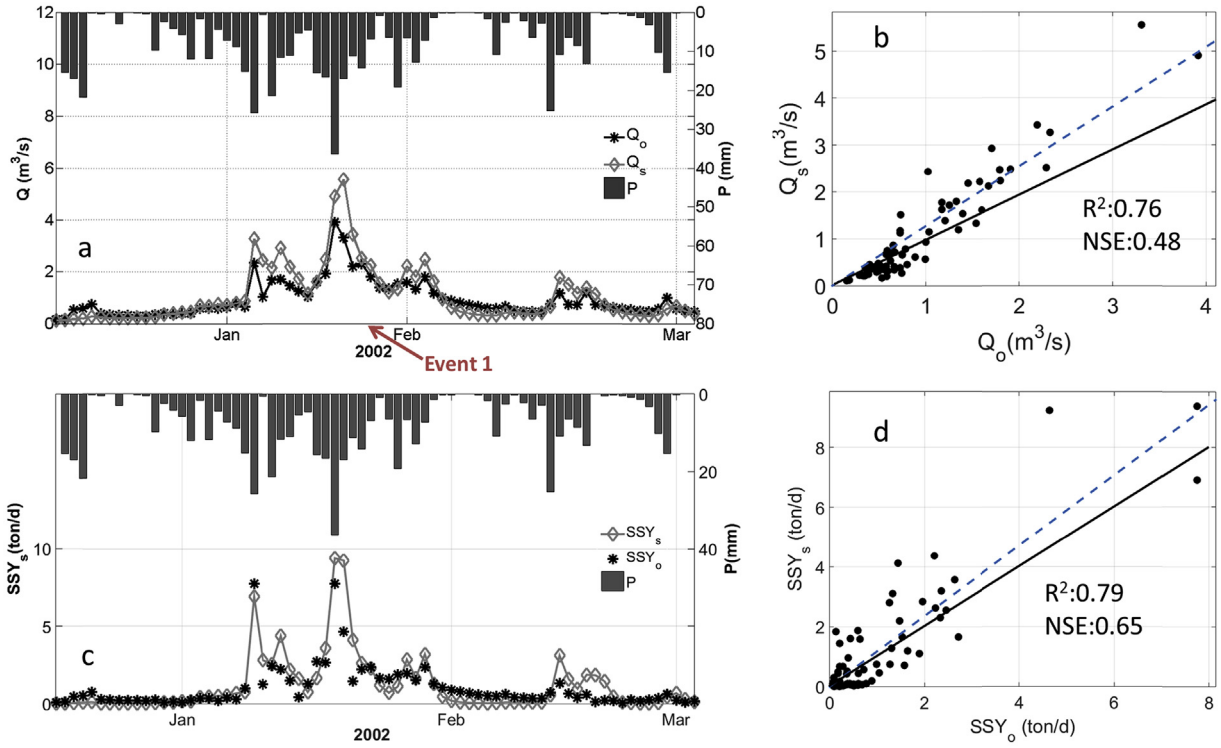

Fig. 5. Model estimates of daily discharge and daily suspended sediment yield (*SSY*) during the calibration period. (a) plot of observed (with subscription 'o') and simulated (with subscription 's') daily average stream flow rate; (b) scatter plot of observed and simulated daily average stream flow rate; (c) plot of observed and simulated daily total *SSY*; (d) scatter plot of observed and simulated daily total *SSY*. Black solid line in panel (b) and (d) is the 1:1 line. Blue dashed line is the best-fit line.(For interpretation of the references to colour in this figure legend,the reader is referred to the web version of this article.).

observed and modeled total suspended sediment losses were 72.76 and 79.94 tons, respectively, for the calibration period. The *RB* was 9.87%. R^2 and *NSE* were 0.79 and 0.65, respectively (Fig. 5c, d). The *RMSE* was 0.83 ton/day (56% of the standard deviation of observed *SSY*) and *IOA* was 0.93. The model performance based on the *NSE*, *IOA*, and *RB* values can be termed as "very good". The *SSY* during the peak flow were overestimated, just like the overestimation of high flows by the hydrologic model.

3.5.3. Validation period

The model was validated using data from Mar 15th, 2002 to the end of 2003. Observed and simulated total discharge per unit area were 1303.8 mm and 1287.7 mm, respectively. The time series of cumulative observed and simulated discharge volume matched each other for most of the period, and the *RB* was only −1.2%. In general, the model reasonably simulated both the timing and magnitude of stream flow during the validation period (*RMSE*: 1.47 mm/day or 56% of the standard deviation of observed discharge; *NSE*: 0.5; and *IOA*: 0.9). However, the model simulation overestimated high flows and underestimated low flows, much like it performed during the calibration period.

The performance of *SSY* simulation registered similar biases as that shown in streamflow simulation. The observed and simulated total annual suspended sediment losses were 170.66 and 132.48 tons, respectively. The total simulated *SSY* for validation period had a relative bias of −22.37%. The erosion model did not miss any erosion events during the validation period. Similar to the flow simulation results, *SSY* estimates were somewhat larger than observed during high flows and smaller during low flows. The *RMSE* was 0.41 ton/day (53% of the observed *SSY*) and the value of *IOA* was 0.86. *NSE* was 0.32. Relatively poor *NSE* is because of the metric's sensitivity to overestimation of *SSY* peaks.

The model performances of flow and *SSY* simulation during calibration and validation periods are summarized in Table 4. The *NSE* and *IOA* values of modeled flow in calibration and validation periods were similar. The *RMSE* of simulated flow in validation period was smaller than in calibration period. The differences between observed and simulated flow rate were smaller during the low flows than high flows. This was partly because of the longer duration of low flow during the validation period. The model performance of suspended sediment simulation in validation period was not as good as in calibration period, even though the performances of flow simulation in both periods were similar. This was due to the bias in the flow simulation and power-law relationship between flow rate and water transport capacity, which exacerbated the *SSY* estimates.

In order to investigate the performance of the integrated model during markedly different flow regimes, a 20-day moving average discharge threshold of 0.2 m^3/s was used to divide the simulation series into wet and dry periods (see Fig. 6a). The total duration of the dry period was 173 days, almost 27% of the two years. The total precipitation during the dry period was 326.6 mm, which is almost 11% of the total precipitation. Table 5 summaries the performances

Table 4
Performance of stream flow and total suspended sediment yield simulation in calibration and validation periods.

	Calibration		Validation	
	Q	*SSY*	*Q*	*SSY*
NSE	0.48	0.65	0.5	0.32
IOA	0.92	0.93	0.9	0.86
RB	15%	9.87%	−1.2%	−22.37%
RMSE	3.03	0.83	1.47	0.41

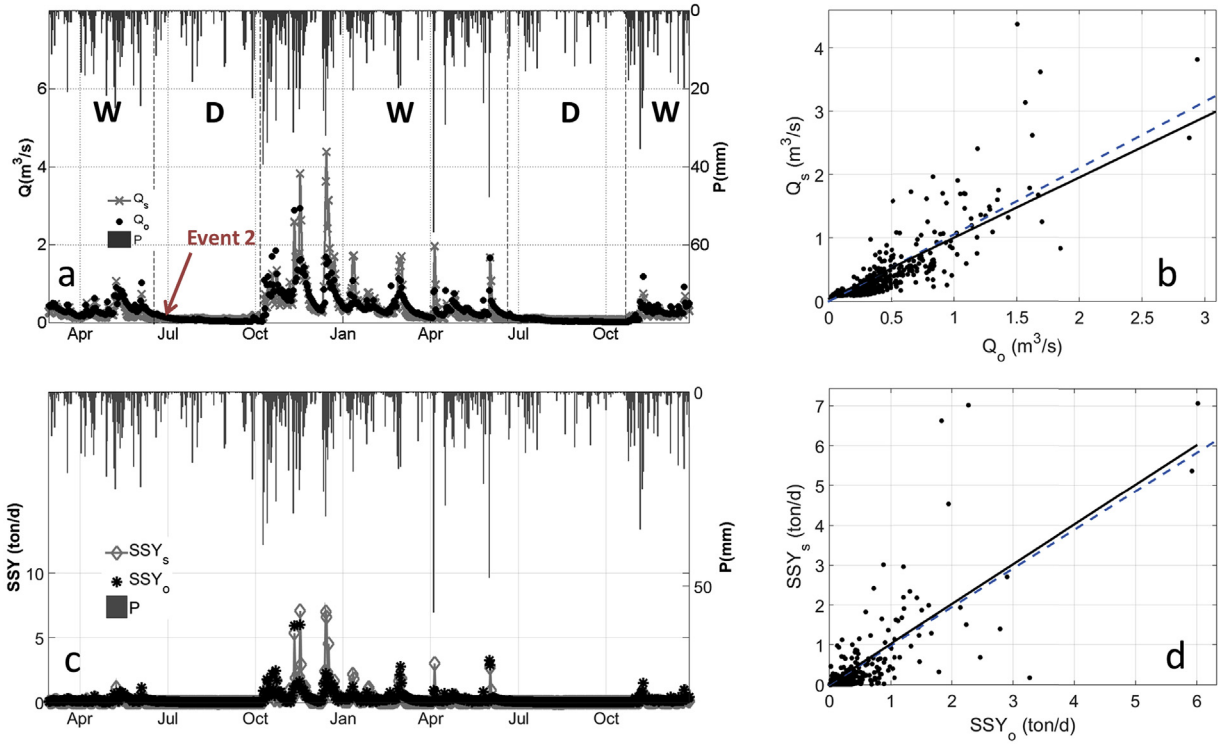

Fig. 6. Model estimates of discharge and suspended sediment yield (*SSY*) during the validation period. (a) plot of observed and simulated daily average stream flow rate. The wet and dry periods were identified by letter 'W' and 'D'; (b) scatter plot of daily average stream flow rate; (c) plot of observed and simulated daily total *SSY*; (d) scatter plot of daily total *SSY*. Black solid line in panel (b) and (d) is the 1:1 line. Blue dashed line is the best-fit line.(For interpretation of the references to colour in this figure legend,the reader is referred to the web version of this article.).

of the integrated model for both flow and *SSY* simulations during wet and dry periods. Both simulations showed better agreement with observed data during wet periods than in dry periods. In general, discharge volume was overestimated for dry periods and underestimated in wet periods, while the *SSY* was underestimated in both wet and dry periods. It is to be noted however that for large peaks, both flow rate and *SSY* was overestimated by the model. The negative *NSE* and *RB* indicate that the calibrated parameter set did not provide accurate enough estimates of flow and *SSY* during dry periods. This is in line with the findings of Jetten et al. (1999) that showed erosion-deposition models cannot guarantee good performance, especially during dry periods, if the events used for calibration are not representative of the prevailing flow regime. It is to be noted that even though the suspended sediment simulation was not good enough during dry period, the bias of suspended sediment is only 9.94% of the total bias.

4. Results and analyses

4.1. Temporal variations in modeled estimates

SSY from the catchment varied markedly from day to day and also non-monotonically with daily precipitation magnitude and intensity (Fig. 7a). The R^2 between observed daily *SSY* and daily rainfall was only 0.14. The R^2 between observed daily *SSY* and the product of daily total rainfall kinetic energy and maximum 30-min rainfall intensity (EI_{30}) was relatively better but still modest, and was equal to 0.53. It is to be noted here that the lagged correlation magnitude between observed daily *SSY* and daily rainfall was maximum for a zero day lag. The large variations in observed daily *SSY* indicate that the daily precipitation magnitude and intensity only have a marginal potential for estimating daily *SSY*. The variation could be because of the non-linear integrated response of the catchment, which may result in generation of markedly different runoff and hence *SSY* for the same daily precipitation amount and EI_{30}. Since runoff generation is directly influenced by the soil moisture in the surface soil layer (which in turn is influenced by meteorological forcings, antecedent hydrologic states, and watershed properties), we explore if the variations in daily *SSY* with EI_{30} could be directly related to the prevailing soil moisture. To this end, data in the *SSY* vs EI_{30} plot are color coded based on simulated daily average soil moisture (Fig. 7a). Based on the first glance, for an identical EI_{30}, *SSY* value appears to be larger for larger catchment-average soil moisture.

To explore this further, two daily events of similar magnitude but with very different moisture conditions were considered (Fig. 8). The first event occurred on 2002/1/27 (identified in Fig. 5) and delivered a total precipitation of 11 mm, a total measured streamflow of 1.3×10^5 m^3 (modelled: 1.8×10^5 m^3) and an event total suspended sediment yield (*SSY*) of 2.1 ton (modelled: 3.4 ton). The second event occurred on 2002/7/2 (identified in Fig. 6) and delivered almost identical rainfall (11.6 mm in total) as the first event, but the total streamflow response and *SSY* at the outlet were much different. Streamflow response for the second event was measured at 1.1×10^4 m^3 (modelled: 1.8×10^4 m^3), while the event

Table 5
Performance of stream flow and suspended sediment simulations in wet and dry periods.

	Q_W	Q_d	SSY_w	SSY_d
NSE	0.33	−0.75	0.25	−1.52
IOA	0.88	0.59	0.85	0.44
RB	4.55%	57.58%	−20.65%	−95.76%
Bias	−56.32	39.15	−34.44	−3.80

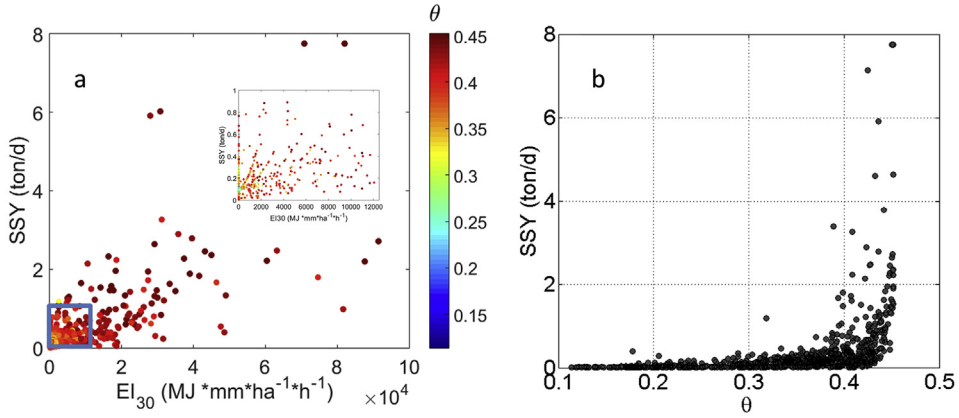

Fig. 7. (a) Scatter plot of daily observed *SSY* and EI_{30}, color coded with daily simulated catchment-average soil moisture; the inset figure is a zoom-in of daily observed *SSY* between 0 and 1 ton/d and EI_{30} between 0–1.2 × 10^4 MJ*mm*ha^{-1}*h^{-1}; (b) Scatter plot of daily observed *SSY* from 2002 to 2003 and daily simulated catchment average soil moisture.

mean *SSY* was 0.066 ton (modelled: 0.054 ton). Notably, even though the rainfall volumes and intensities were similar for these two selected events, the first event lead to much larger runoff and *SSY* at the outlet (Fig. 8a). The difference was mostly because of strong contrast in the antecedent moisture condition between the two cases (Fig. 8c and f). Around 88% of the catchment area was saturated at the start of event 1, with this fraction increasing to around 98% during the event. As a result almost the entire catchment participated in runoff generation leading to larger soil loss and larger mean *SSY*. This is not surprising as the catchment is fairly small. In contrast, only around 18% of the catchment area was saturated before event 2 and the fraction increased to around 36% during the event. Fig. 9b and d further reinforces the narrative that surface soil moisture influences *SSY* as it shows that event responses (both streamflow and *SSY*) were negligible for events from day-of-year (*DOY*) 200 to 290 in 2002, as the soil moisture was generally below saturation during this period (Fig. 9c). By day 290, the water table was near the soil surface, which resulted in any additional precipitation to cause saturation excess runoff. To evaluate the variation of *SSY* with soil moisture across all events, a scatter plot between *SSY* and spatially averaged moisture conditions in the top soil layer (of thickness = 10 cm) was drawn (Fig. 7b). The figure suggests that runoff generation (from saturation excess or infiltration excess) and hence erosion per unit event magnitude is indeed larger when the top soil layer in the catchment is near saturation. These results suggest that accurate prediction of spatial distribution of soil moisture is critical for generating temporally fine estimates of *SSY*. Notably, increase in soil saturation also

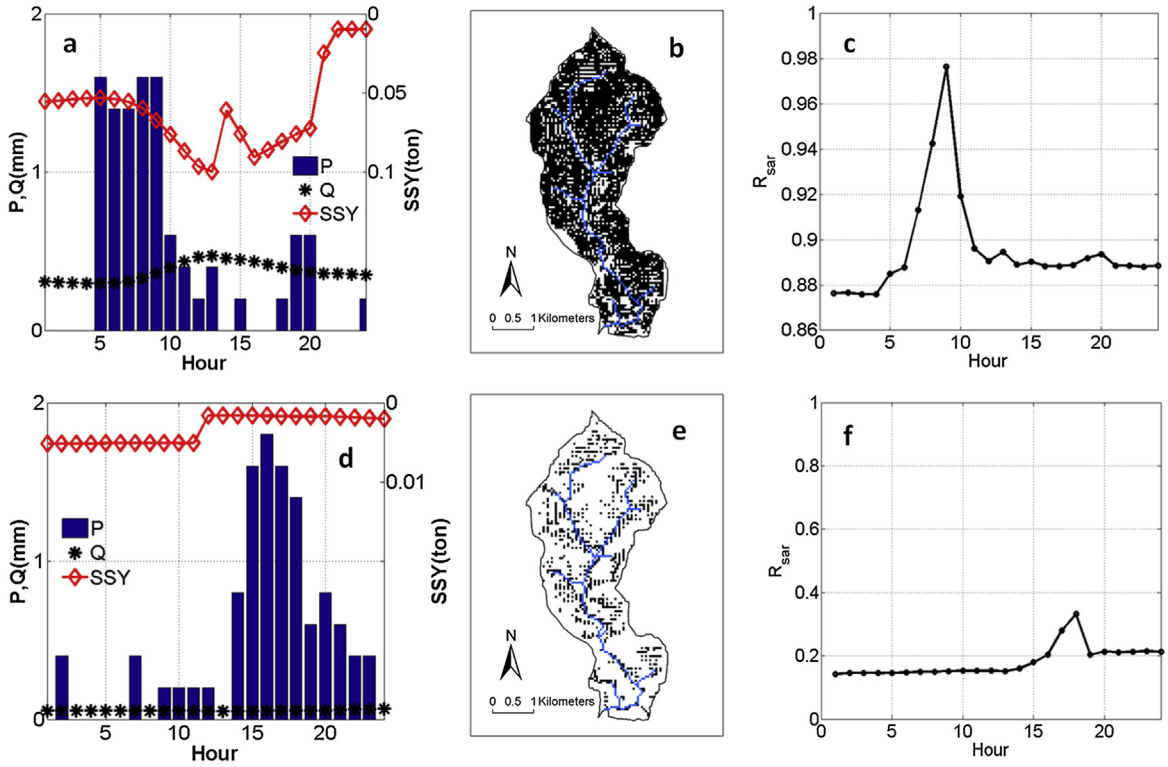

Fig. 8. The hourly rainfall, observed discharge and *SSY* of two selected events (a,d); the simulated spatial distribution of soil loss area for two selected events (b,e), area with soil losses were black; the changes of saturated ratio of the simulated first layer soil moisture of the whole catchment (e,f); the plots for first event were on the top.

increases soil cohesion which in turn may reduce erosion (see Equation (7)), but its impact is negated by large runoff generation for higher soil saturation cases. It is to be noted that the soil saturation of the top soil layer is a function of coupled surface water-groundwater-evapotranspiration interactions, and the parameters (such as topography, subsurface soil property, land cover etc.) that influence these processes. As such, the expressed role of surface soil moisture on *SSY* indirectly highlights the need for modeling of coupled processes in both space and time, much along the lines of process representations implemented in GEOtop.

Suspended sediment yield from the catchment also showed ample variations between wet and dry periods. Even though the wet period (see Fig. 6a) spanned only around 73% of the simulation time, it delivered 98.4% (99.9%, modeled) of the total sediment yield. This is in line with previously reported results from both field (Fu, 1989) and modeling experiments (Baartman et al., 2012; Zhang et al., 2012) that have shown that a few extreme events may contribute to a large portion of annual total soil erosion. Notably, our research area has a temperate weather and lacks extreme precipitation events, but nonetheless the dry period (~27% of the total simulation time) delivered only ~1% of the total *SSY*.

4.2. Spatially distributed estimates of erosion and deposition

Estimates of erosion and deposition simulated by the model displayed significant heterogeneity in both space and time. For example, for the two selected precipitation events with similar amounts of rainfall (Fig. 8a, d), the areal extent of soil loss and its spatial distribution locations were very different (Fig. 8b, e). The percentage area that participated in erosion loss was as high as 72% in event 1, while reaching only around 14% for event 2. Similarly the areal fraction of deposition areas were 14% and 7% respectively for the two events. A larger erosion loss area for event 1 can again be attributed to higher antecedent surface soil moisture in the catchment, which leads to a larger fraction of catchment area generating runoff. A larger volume of overland flow resulted in, higher shear stress and hence more soil loss from larger area. For the two years, the mean areal fraction of erosion and deposition was 27% and 8% respectively. Both erosion and deposition areal fraction were larger in wet periods than in dry periods. The variations of erosion and deposition areal portion were larger in wet periods (Table 6). Notably, the erosion and deposition areal fractions in the catchment were as large as 79% and 36% of the catchment area during the two year simulation periods. These statistics highlight that the source and sink areas in a catchment are very dynamic and change at both event and seasonal scales. Also, given the role of soil saturation area on runoff/erosion generation, dynamic mapping of source/sink areas can benefit from spatially-explicit simulations of coupled hydrologic processes.

At the annual scale, most deposition occurred near the riparian zone of the stream (dark blue color in Fig. 10a), due to its relatively flat topography. Erosive losses were mainly located in the transition area between the hillslope and the riparian zone (dark red color in Fig. 10a), which had both large flow accumulation area and relatively steep slope. The locations of erosion and deposition in terms of slope and specific catchment area are shown in Fig. 10c and d. Specific catchment area is the ratio of total contributing area of each land pixel and the pixel's width perpendicular to the flow direction. The bar plot of average erosion/deposition per unit area for different specific catchment areas shows that in general, erosion and deposition rates per unit area were larger with increasing specific catchment area. Areas with larger contributing areas generally had larger overland flow and hence larger transport capacity thus allowing more entrainment of soil particles (Fig. 10c). Additionally, as more suspended sediment was transported to areas with large contribution area, the possibility that the suspended sediment concentration (*SSC*) exceeded the transport capacity, especially at flatter locations, also increased. This explains the increase in deposition with larger contributing areas (Fig. 10d). Notably, total simulated soil erosive losses per unit area (*Es*) did not show a monotonic trend with slope (Fig. 10c). For flatter slopes, *Es* is expected to be small because of the lower flow velocities. For larger slopes, while the local erosion at the cell under consideration is expected to be large, the incoming sediment input may either be small or large for a given contributing area depending on the spatio-temporal extent of soil saturation area that determines runoff generation. As a result, *Es*, which is an integrated net-erosional response from the contributing area and the pixel

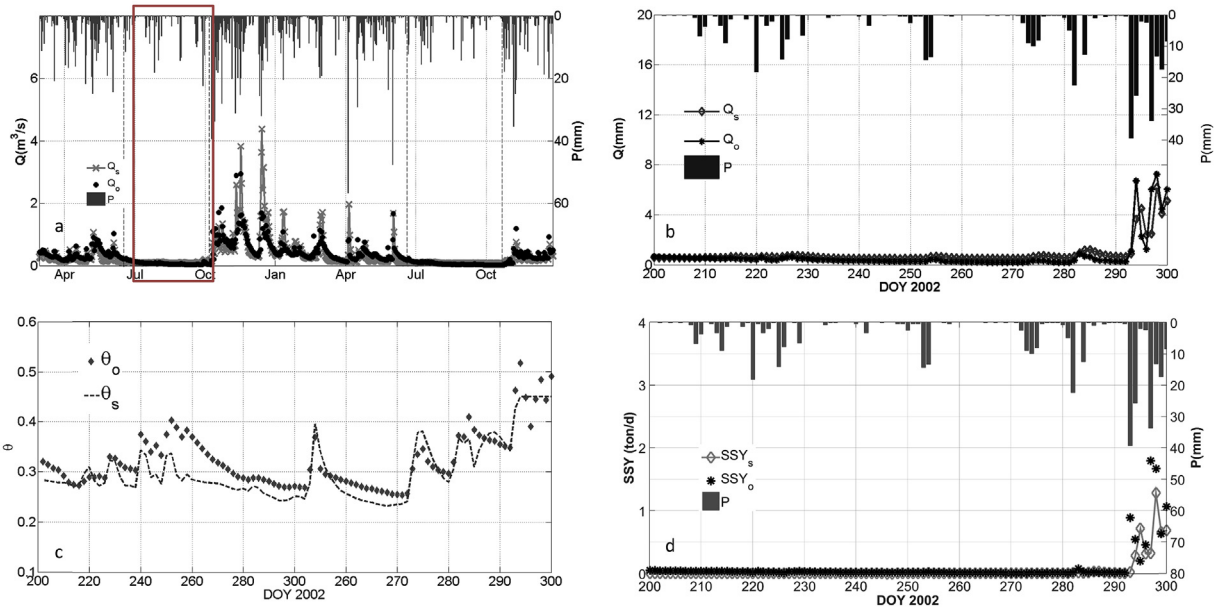

Fig. 9. (a) the integrated model is able to capture occurrence of runoff events after a dry periods. The red box identifies the periods used in panel b, c, and d; (b)observed and simulated discharge per unit area; (c). observed and simulated soil moisture (top 25 cm) (d)observed and simulated daily *SSY*.

Table 6
The mean and standard deviation of erosion and deposition areas.

	Mean erosional area fraction	Mean depositional area fraction	Standard deviation of erosional area fraction	Standard deviation of depositional area fraction
2002–2003	0.27	0.08	0.246	0.0859
Wet periods	0.33	0.11	0.2476	0.0835
Dry periods	0.11	0.02	0.1519	0.0585

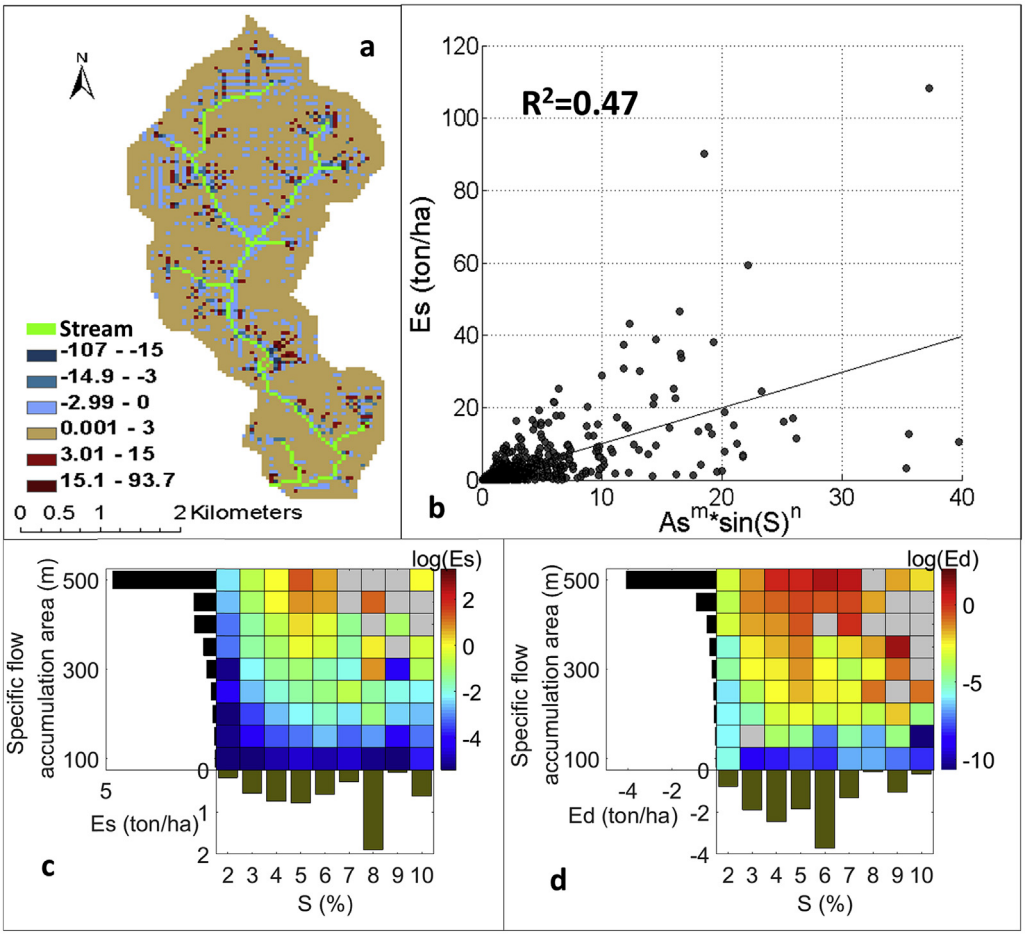

Fig. 10. (a) Spatial map of soil erosion and deposition for each land pixel (unit:ton/ha/yr) for the entire two year simulation period; (b) Scatter plot between erosive loss (*Es*) and slope-length factor for each land pixel; (c) Color chart of the logarithm of simulated erosive loss (log (ton)) for a range of slope (on x-axis) and specific flow accumulation area (on y-axis). Also included on the two axes are the bar plots of total erosive losses per unit area for different slope and specific catchment area classes; (d) Color chart of the logarithm of simulated deposition (log (ton)). Also included on the two axes are the bar plots of total deposition per unit area for different slope and specific catchment area classes. Note: grey cells in (c) and (d) are used to identify joint classes with no data.

under consideration, may show non-monotonic variation with slope. This non-monotonic variation also has a tangible impact on the relation between the length-slope (*LS*) factor and the total simulated soil erosive losses per unit area (*Es*). Model results suggest that while *Es* shows an overall increasing trend with *LS* (Fig. 10b), the relation is not one to one, and shows ample variations around the *Es*-*LS* line ($R^2 = 0.47$, $\sigma^2 = 5.44$). While the result is based on only two years of simulation, it does highlight that the source efficiency or the erosion rates (in homogeneous watersheds/hillslopes with uniform soil property) is not just a simple function of contribution area and slope, and can be strongly influenced by the dynamic spatio-temporal distribution of soil moisture conditions.

5. Summary and conclusions

In this study, we developed an open-source sediment erosion/deposition module for a 3D surface-subsurface hydrologic model, GEOtop, and evaluated its applicability in explaining the spatio-temporal distribution of erosion, deposition, and sediment yield dynamics at both plot and catchment scale. The model uses a physically-based representation of coupled surface-subsurface hydrologic processes and a comprehensive land-surface energy and water interaction scheme to simulate hydrologic response and consequent sediment dynamics. Because of its fully distributed nature, the model can account for spatial heterogeneity in the watershed. As the model runs at an adaptive time interval determined by the dynamics of states, it can be used to perform simulations at event to inter-decadal scales. At the plot level, the model was evaluated at event time scale. Results show that the model was able to capture both the trend and the quantity of runoff and suspended sediment concentration (SSC) in response to events of varying intensity and duration. At the catchment level, after

performing a global multivariate sensitivity analyses to identify sensitive parameters for hydrologic modeling (such as leaf area index, rill width ratio, depth of the first soil layer, Chezy's roughness coefficient, and vertical hydraulic conductivity of the first soil layer) and sediment dynamics (such as Chezy's roughness coefficient, soil median particle size, and rill width ratio), the model performance was evaluated at daily and seasonal time scales. In general, the model reasonably simulated both the timing and magnitude of stream flow and suspended sediment yield (*SSY*) from the catchment. Both streamflow and suspended sediment yield simulations showed better agreement with observed data during wet periods than in dry periods. The discharge volume was overestimated for dry periods and underestimated in wet periods, while the *SSY* was underestimated in both wet and dry periods. Notably, the biases in suspended sediment yield simulation were similar to that shown in streamflow simulation, thus highlighting that accuracy of flow simulations critically influences the estimation accuracy of *SSY*. While our research area has a temperate maritime climate and lacks extreme precipitation events, but still dry period (~27% of the total simulation time) delivered only ~1% of the *SSY*. This underscores the importance of obtaining robust calibration parameter sets that at least perform well during wet periods, as is well documented in nutrient export studies (Jordan et al., 2005; Nasr et al., 2007; Ye et al., 2012). It is to be noted that the sensitivity analysis performed for Dripsey catchment could serve as a reference for future model applications, and for prioritizing observation of parameters to reduce the uncertainties in the erosion model.

Observed *SSY* from the catchment showed a non-monotonic variation with daily precipitation magnitude. Further examination of simulation results revealed that *SSY* per unit event magnitude varied proportionally with the prevailing soil moisture. The result indicates that accurate prediction of spatial distribution of soil moisture is critical for generating temporally fine estimates of *SSY*. Larger *SSY* per unit event magnitude for higher soil saturation also indicates that large runoff generation for wetter soil moisture conditions negated the impact of increase in soil cohesion with moisture content. The simulation results also showed that the source (erosion) and sink (deposition) areas in a catchment were heterogeneous and dynamic, and could change from one event to the next. Again, the extent of source/sink areas were found to be influenced by prevailing moisture conditions, which in turn determined the quantity of runoff generation. Model results also suggest that long-term erosion rate from a location was not a simple function of slope-length. In fact, the relation between erosion and slope-length showed ample variations, thus highlighting that the source efficiency or the erosion rates (in homogeneous catchments/hillslopes with same rainfall forcing and uniform soil property) can be severely influenced by the dynamic spatio-temporal distribution of soil moisture conditions. Since the spatio-temporal dynamics of soil moisture is dependent on coupled process interactions such as evapo-transpiration, capillary rise and lateral groundwater flow, aforementioned results make a compelling case for spatially-explicit simulations of coupled hydrologic processes for estimation of erosion/deposition distribution and sediment generation.

The simulation results presented in this study do not account for uncertainty in parameters. Also, even though the parameters in the presented model are physically-based and can be obtained through measurements, because of the sparseness of observed data, disconnect between observation and model scale, and model uncertainty, these parameters still need to be calibrated. This is a big challenge for spatially-distributed models such as GEOtopSed, as they are computationally demanding. Further confidence in the modeled estimates could be built by obtaining field estimates of states (e.g. ground water, residence time etc.) and related parameters (e.g. rill width, soil cohesion etc.), and by implementing the model in varied settings. The presented model version does not account for bank-erosion processes, which limits its applicability to watersheds with small bank erosion w.r.t. total hillslope losses. It is to be noted that 1D representation of flow routing in channel especially limits the calculation of lateral convective gradients and shear, thus hindering the development of a comprehensive sediment erosion and transport module. Also, as the GEOtop model uses kinematic wave scheme to solve for overland and channel flow, the model is not well suited for flow and sediment yield calculations in flow regimes with either Froude number smaller than 0.5 or kinematic wave number smaller than 5 (Vieira, 1983). For using the model as a predictive tool, vegetation dynamics in response to changes in meteorological forcings and hydrologic states need to be accounted for. In spite of aforementioned limitations, the open-source integrated modeling framework presented here offers the potential for its use both as an evaluation and retrospective-prediction tool, and as a virtual laboratory for understanding the role of hydrologic states and parameters on sediment dynamics.

Acknowledgements

We appreciate the valuable feedbacks from reviewers and the editor, which greatly improved this manuscript. This study was supported by the Irish Environmental Protection Agency (EPA) under the Science Technology Research & Innovation for the Environment (STRIVE) Programme 2007–2013 of Ireland (Soil H: Interactions of soil hydrology, land use and climate change and their impact on soil quality; 2007–S-SL-2-S1). Mukesh Kumar acknowledges the support of National Science Foundation CZO grant (EAR-1331846). We acknowledge the developers of GEOtop model, for keeping the software open-source and free.

References

Albertson, J.D., Kiely, G., 2001. On the structure of soil moisture time series in the context of land surface models. J. Hydrol. 243, 101–119. http://dx.doi.org/10.1016/s0022-1694(00)00405-4.

Baartman, J.E.M., Jetten, V.G., Ritsema, C.J., de Vente, J., 2012. Exploring effects of rainfall intensity and duration on soil erosion at the catchment scale using openLISEM: Prado catchment, SE Spain. Hydrol. Process. 26, 1034–1049. http://dx.doi.org/10.1002/hyp.8196.

Bertoldi, G., 2004. The water and energy balance at basin scale: a distributed modeling approach. Environmental Engineering, University of Trento, p. 202.

Bertoldi, G., Della Chiesa, S., Notarnicola, C., Pasolli, L., Niedrist, G., Tappeiner, U., 2014. Estimation of soil moisture patterns in mountain grasslands by means of SAR RADARSAT2 images and hydrological modeling. J. Hydrol. 516, 245–257. http://dx.doi.org/10.1016/j.jhydrol.2014.02.018.

Bullock, M.S., Kemper, W., Nelson, S., 1988. Soil cohesion as affected by freezing, water content, time and tillage. Soil Sci. Soc. Am. J. 52, 770–776.

Cabral, M.C., Garrote, L., Bras, R.L., Entekhabi, D., 1992. A kinematic model of infiltration and runoff generation in layered and sloped soils. Adv. Water Resour. 15, 311–324. http://dx.doi.org/10.1016/0309-1708(92)90017-V.

Chen, X., Kumar, M., McGlynn, B.L., 2014. Variations in streamflow response to large Hurricane-season storms in a southeastern U.S. Watershed. J. Hydrometeorol. 16, 55–69. http://dx.doi.org/10.1175/JHM-D-14-0044.1.

de Vente, J., Poesen, J., Verstraeten, G., Van Rompaey, A., Govers, G., 2008. Spatially distributed modelling of soil erosion and sediment yield at regional scales in Spain. Glob. Planet. Change 60, 393–415. http://dx.doi.org/10.1016/j.gloplacha.2007.05.002.

Della Chiesa, S., Bertoldi, G., Niedrist, G., Obojes, N., Endrizzi, S., Albertson, J.D., Wohlfahrt, G., Hörtnagl, L., Tappeiner, U., 2014. Modelling changes in grassland hydrological cycling along an elevational gradient in the Alps. Ecohydrol. 7, 1453–1473. http://dx.doi.org/10.1002/eco.1471.

DeRoo, A.P.J., Wesseling, C.G., Ritsema, C.J., 1996. LISEM: a single-event physically based hydrological and soil erosion model for drainage basins .1. Theory, input and output. Hydrol. Process. 10, 1107–1117.

Endrizzi, S., Gruber, S., Dall'Amico, M., Rigon, R., 2014. GEOtop 2.0: simulating the combined energy and water balance at and below the land surface accounting for soil freezing, snow cover and terrain effects. Geosci. Model Dev. 7, 2831–2857. http://dx.doi.org/10.5194/gmd-7-2831-2014.

Fernandez, G.P., Chescheir, G.M., Skaggs, R.W., Amatya, D.M., 2005. Development and testing of watershed-scale models for poorly drained soils. Trans. ASAE 48,

639–652.
Foster, G., Yoder, D., Weesies, G., McCool, D., McGregor, K., Bingner, R., 2005. Revised Universal Soil Loss Equation Version 2. Science Documentation. (Draft). USDA-ARS.
Franks, S.W., Beven, K.J., Quinn, P.F., Wright, I.R., 1997. On the sensitivity of soil-vegetation-atmosphere transfer (SVAT) schemes: equifinality and the problem of robust calibration. Agric. For. Meteorol. 86, 63–75. http://dx.doi.org/10.1016/S0168-1923(96)02421-5.
Fu, B., 1989. Soil erosion and its control in the loess plateau of China. Soil Use Manag. 5, 76–82. http://dx.doi.org/10.1111/j.1475-2743.1989.tb00765.x.
Ghimire, C.P., Bonell, M., Bruijnzeel, L.A., Coles, N.A., Lubczynski, M.W., 2013. Reforesting severely degraded grassland in the Lesser Himalaya of Nepal: effects on soil hydraulic conductivity and overland flow production. J. Geophys. Res. Earth Surf. 118, 2528–2545. http://dx.doi.org/10.1002/2013JF002888.
Golubev, G.N., 1982. Soil erosion and agriculture in the world: an assessment and hydrological implications. Hydrol. Sci. J. – J. Des. Sci. Hydrol. 27, 243–243.
Govers, G., 1990. Empirical Relationships for the Transport Capacity of Overland Flow. IAHS Publication, IAHS Press, Institute of Hydrology, pp. 45–63.
Vorst, HAvd, 1992. BI-CGSTAB: a fast and smoothly converging variant of BI-CG for the solution of nonsymmetric linear systems. SIAM J. Sci. Stat. Comput. 13, 631–644. http://dx.doi.org/10.1137/0913035.
Heppner, C.S., Ran, Q., VanderKwaak, J.E., Loague, K., 2006. Adding sediment transport to the integrated hydrology model (InHM): development and testing. Adv. Water Resour. 29, 930–943. http://dx.doi.org/10.1016/j.advwatres.2005.08.003.
Heppner, C.S., Loague, K., VanderKwaak, J.E., 2007. Long-term InHM simulations of hydrologic response and sediment transport for the R-5 catchment. Earth Surf. Process. Landforms 32, 1273–1292. http://dx.doi.org/10.1002/esp.1474.
Hessel, R., van den Bosch, R., Vigiak, O., 2006. Evaluation of the LISEM soil erosion model in two catchments in the East African Highlands. Earth Surf. Process. Landforms 31, 469–486. http://dx.doi.org/10.1002/esp.1280.
Hessell, R., 2005. Effects of grid cell size and time step length on simulation results of the Limburg soil erosion model (LISEM). Hydrol. Process. 19, 3037–3049. http://dx.doi.org/10.1002/hyp.5815.
Hueso-González, P., Ruiz-Sinoga, J., Martínez-Murillo, J., Lavee, H., 2015. Overland flow generation mechanisms affected by topsoil treatment: application to soil conservation. Geomorphology 228, 796–804.
Ivanov, V.Y., Vivoni, E.R., Bras, R.L., Entekhabi, D., 2004. Catchment hydrologic response with a fully distributed triangulated irregular network model. Water Resour. Res. 40 http://dx.doi.org/10.1029/2004WR003218.
Jain, M., Kothyari, U., Raju, K., 2005. Gis based distributed model for soil erosion and rate of sediment outflow from catchments. J. Hydraulic Eng. 131, 755–769. http://dx.doi.org/10.1061/(ASCE)0733-9429(2005)131:9(755).
Jetten, V., de Roo, A., Favis-Mortlock, D., 1999. Evaluation of field-scale and catchment-scale soil erosion models. CATENA 37, 521–541. http://dx.doi.org/10.1016/S0341-8162(99)00037-5.
Jordan, P., Menary, W., Daly, K., Kiely, G., Morgan, G., Byrne, P., Moles, R., 2005. Patterns and processes of phosphorus transfer from Irish grassland soils to rivers—integration of laboratory and catchment studies. J. Hydrol. 304, 20–34. http://dx.doi.org/10.1016/j.jhydrol.2004.07.021.
Jost, G., Schume, H., Hager, H., Markart, G., Kohl, B., 2012. A hillslope scale comparison of tree species influence on soil moisture dynamics and runoff processes during intense rainfall. J. Hydrol. 420, 112–124.
Julien, P., Simons, D., 1985. Sediment transport capacity of overland flow. Trans. ASAE 28, 755–762.
Kim, J., Ivanov, V.Y., Katopodes, N.D., 2013. Modeling erosion and sedimentation coupled with hydrological and overland flow processes at the watershed scale. Water Resour. Res. 49, 5134–5154. http://dx.doi.org/10.1002/wrcr.20373.
Krause, P., Boyle, D., Bäse, F., 2005. Comparison of different efficiency criteria for hydrological model assessment. Adv. Geosciences 5, 89–97.
Kumar, M., Duffy, C.J., Salvage, K.M., 2009. A second-order accurate, finite volume–based, integrated hydrologic modeling (FIHM) framework for simulation of surface and subsurface flow. Vadose Zone J. 8, 873–890. http://dx.doi.org/10.2136/vzj2009.0014.
Legates, D.R., Mahmood, R., Levia, D.F., DeLiberty, T.L., Quiring, S.M., Houser, C., Nelson, F.E., 2011. Soil moisture: a central and unifying theme in physical geography. Prog. Phys. Geogr. 35, 65–86.
Lewis, C., 2003. Phosphorus, Nitrogen and Suspended Sediment Loss from Soil to Water from Agricultural Grassland. Department of Civil and Environmental Engineering, University College Cork.
Lewis, C., 2011. Measurement and Modelling of Soil Hydrological Properties for Use in the Distributed Rainfall Runoff Model - GEOtop. Department of Civil and Environmental Engineering, University College Cork.
Lewis, C., Albertson, J., Xu, X., Kiely, G., 2012. Spatial variability of hydraulic conductivity and bulk density along a blanket peatland hillslope. Hydrol. Process. 26, 1527–1537. http://dx.doi.org/10.1002/hyp.8252.
Lewis, C., Albertson, J., Zi, T., Xu, X., Kiely, G., 2013. How does afforestation affect the hydrology of a blanket peatland? A modelling study. Hydrol. Process. 27, 3577–3588.
Mati, B.M., Morgan, R.P.C., Quinton, J.N., 2006. Soil erosion modelling with EUROSEM at Embori and Mukogodo catchments, Kenya. Earth Surf. Process. Landforms 31, 579–588. http://dx.doi.org/10.1002/esp.1347.
Miguez-Macho, G., Fan, Y., 2012. The role of groundwater in the Amazon water cycle: 1. Influence on seasonal streamflow, flooding and wetlands. J. Geophys. Res. Atmos. 117 (1984–2012).
Montaldo, N., Toninelli, V., Albertson, J.D., Mancini, M., Troch, P.A., 2003. The effect of background hydrometeorological conditions on the sensitivity of evapotranspiration to model parameters: analysis with measurements from an Italian alpine catchment. Hydrol. Earth Syst. Sci. 7, 848–861. http://dx.doi.org/10.5194/hess-7-848-2003.
Morgan, R.P.C., Quinton, J.N., Smith, R.E., Govers, G., Poesen, J.W.A., Auerswald, K., Chisci, G., Torri, D., Styczen, M.E., 1998. The European Soil Erosion Model (EUROSEM): a dynamic approach for predicting sediment transport from fields and small catchments. Earth Surf. Process. Landforms 23, 527–544.
Moriasi, D., Arnold, J., Van Liew, M., Bingner, R., Harmel, R., Veith, T., 2007. Model evaluation guidelines for systematic quantification of accuracy in watershed simulations. Trans. ASABE 50, 885–900.
Nash, J.E., Sutcliffe, J.V., 1970. River flow forecasting through conceptual models part I — A discussion of principles. J. Hydrol. 10, 282–290. http://dx.doi.org/10.1016/0022-1694(70)90255-6.
Nasr, A., Bruen, M., Jordan, P., Moles, R., Kiely, G., Byrne, P., 2007. A comparison of SWAT, HSPF and SHETRAN/GOPC for modelling phosphorus export from three catchments in Ireland. Water Res. 41, 1065–1073. http://dx.doi.org/10.1016/j.watres.2006.11.026.
Niu, G.-Y., Pasetto, D., Scudeler, C., Paniconi, C., Putti, M., Troch, P., DeLong, S., Dontsova, K., Pangle, L., Breshears, D., 2014. Incipient subsurface heterogeneity and its effect on overland flow generation–insight from a modeling study of the first experiment at the biosphere 2 landscape evolution observatory. Hydrol. Earth Syst. Sci. 18, 1873–1883.
Orchard, C.M., Lorentz, S.A., Jewitt, G.P.W., Chaplot, V.A.M., 2013. Spatial and temporal variations of overland flow during rainfall events and in relation to catchment conditions. Hydrol. Process. 27, 2325–2338. http://dx.doi.org/10.1002/hyp.9217.
Penna, D., Tromp-van Meerveld, H., Gobbi, A., Borga, M., Dalla Fontana, G., 2011. The influence of soil moisture on threshold runoff generation processes in an alpine headwater catchment. Hydrol. Earth Syst. Sci. 15, 689–702.
Ramsankaran, R., Kothyari, U.C., Ghosh, S.K., Malcherek, A., Murugesan, K., 2013. Physically-based distributed soil erosion and sediment yield model (DREAM) for simulating individual storm events. Hydrol. Sci. J. 58, 872–891. http://dx.doi.org/10.1080/02626667.2013.781606.
Ran, Q., Su, D., Li, P., He, Z., 2012. Experimental study of the impact of rainfall characteristics on runoff generation and soil erosion. J. Hydrol. 424, 99–111.
Renard, K.G., Foster, G.R., Weesies, G.A., Porter, J.P., 1991. RUSLE: revised universal soil loss equation. J. Soil Water Conserv. 46, 30–33.
Rigon, R., Bertoldi, G., Over, T.M., 2006. GEOtop: a distributed hydrological model with coupled water and energy budgets. J. Hydrometeorol. 7, 371–388.
Rosenberg, E., Clark, E., Steinemann, A., Lettenmaier, D., 2013. On the contribution of groundwater storage to interannual streamflow anomalies in the Colorado River basin. Hydrol. Earth Syst. Sci. 17, 1475–1491.
Safeeq, M., Mauger, G.S., Grant, G.E., Arismendi, I., Hamlet, A.F., Lee, S.-Y., 2014. Comparing large-scale hydrological model predictions with observed streamflow in the Pacific northwest: effects of climate and groundwater*. J. Hydrometeorol. 15, 2501–2521.
Simoni, S., Zanotti, F., Bertoldi, G., Rigon, R., 2008. Modelling the probability of occurrence of shallow landslides and channelized debris flows using GEOtop-FS. Hydrol. Process. 22, 532–545. http://dx.doi.org/10.1002/hyp.6886.
Singh, J., Knapp, H.V., Arnold, J., Demissie, M., 2005. Hydrological modeling of the Iroquois River watershed using HSPF and SWAT. J. Am. Water Resour. Assoc. 41, 343–360.
Smith, R.E., Goodrich, D.C., Quinton, J.N., 1995. Dynamic, distributed simulation of watershed erosion: the KINEROS2 and EUROSEM models. J. Soil Water Conserv. 50, 517–520.
Tao, J., Barros, A.P., 2014. Coupled prediction of flood response and debris flow initiation during warm- and cold-season events in the Southern Appalachians, USA. Hydrol. Earth Syst. Sci. 18, 367–388. http://dx.doi.org/10.5194/hess-18-367-2014.
VanderKwaak, J.E., Loague, K., 2001. Hydrologic-Response simulations for the R-5 catchment with a comprehensive physics-based model. Water Resour. Res. 37, 999–1013. http://dx.doi.org/10.1029/2000WR900272.
Vieira, J.H.D., 1983. Conditions governing the use of approximations for the Saint-Vénant equations for shallow surface water flow. J. Hydrol. 60, 43–58. http://dx.doi.org/10.1016/0022-1694(83)90013-6.
von Freyberg, J., Rao, P.S.C., Radny, D., Schirmer, M., 2015. The impact of hillslope groundwater dynamics and landscape functioning in event-flow generation: a field study in the Rietholzbach catchment. Switz. Hydrogeol. J. 1–14.
Warner, S., Kiely, G., Morgan, G., O'Halloran, J., 2009. Does quantifying antecedent flow conditions improve stream phosphorus export estimation? J. Hydrol. 378, 97–104. http://dx.doi.org/10.1016/j.jhydrol.2009.09.009.
Wicks, J.M., Bathurst, J.C., 1996. SHESED: a physically based, distributed erosion and sediment yield component for the SHE hydrological modelling system. J. Hydrol. 175, 213–238. http://dx.doi.org/10.1016/s0022-1694(96)80012-6.
Willmott, C.J., 1981. On the validation of models. Phys. Geogr. 2, 184–194.
Wischmeier, W.H., Smith, D.D., 1978. Predicting Rainfall Erosion Losses: a Guide to Conservation Planning. Dept. of Agriculture, Science and Education Administration: for sale by the Supt. of Docs., US Govt. Print. Off.
Wu, T.H., McKinnell Iii, W.P., Swanston, D.N., 1979. Strength of tree roots and landslides on Prince of Wales Island, Alaska. Can. Geotechnical J. 16, 19–33. http://dx.doi.org/10.1139/t79-003.
Yang, C.T., 1972. Unit stream power and sediment transport. J. Hydraulics Div. 98, 1805–1826.

Ye, S., Covino, T.P., Sivapalan, M., Basu, N.B., Li, H.-Y., Wang, S.-W., 2012. Dissolved nutrient retention dynamics in river networks: a modeling investigation of transient flows and scale effects. Water Resour. Res. 48 http://dx.doi.org/10.1029/2011WR010508.

Zhang, Y., Hernandez, M., Anson, E., Nearing, M.A., Wei, H., Stone, J.J., Heilman, P., 2012. Modeling climate change effects on runoff and soil erosion in southeastern Arizona rangelands and implications for mitigation with conservation practices. J. Soil Water Conserv. 67, 390–405. http://dx.doi.org/10.2489/jswc.67.5.390.

Zimmermann, A., Schinn, D.S., Francke, T., Elsenbeer, H., Zimmermann, B., 2013. Uncovering patterns of near-surface saturated hydraulic conductivity in an overland flow-controlled landscape. Geoderma 195–196, 1–11. http://dx.doi.org/10.1016/j.geoderma.2012.11.002.